Available online at www.sciencedirect.com
ScienceDirect
Ceramics International 37 (2011) 971–977
CERAMICS INTERNATIONAL
www.elsevier.com/locate/ceramint

Synthesis and microstructural characterization of nano-size calcium phosphates with different stoichiometry

Celaletdin Ergun [a,*], Zafer Evis [b], Thomas J. Webster [c], Filiz Cinar Sahin [d]

[a] Istanbul Technical University, Department of Mechanical Engineering, Taksim, Istanbul 34437, Turkey
[b] Middle East Technical University, Department of Engineering Sciences, Ankara 06531, Turkey
[c] Brown University, Division of Engineering and Department of Orthopaedics, Providence, RI 02912, USA
[d] Istanbul Technical University, Department of Metallurgical and Materials Engineering, Maslak, Istanbul 34469, Turkey

Received 12 August 2010; received in revised form 15 September 2010; accepted 2 November 2010
Available online 1 December 2010

Abstract

Calcium phosphates with Ca/P molar ratios of 0.5, 0.75, 1.33, 1.5, 1.55, 1.67, 2.0, and 2.5 were synthesized by a wet chemistry precipitation method and sintered at 500 °C, 700 °C, 900 °C, 1100 °C and 1300 °C for 2 h. Presence of phases and microstructures of calcium phosphates were determined by X-ray diffraction and scanning electron microscopy. In all different Ca/P ratios, the precipitated phase was always hydroxyapatite with very small size and/or partial disorderness regardless of the Ca/P ratios in the starting precipitating medium. For samples with 0.5 and 0.75 Ca/P ratios in starting solution, tricalcium phosphate and calcium pyrophosphate phases were observed. In contrast, for samples with 1.0 and 1.33 Ca/P ratios, the only stable phase was tricalcium phosphate. For the samples with Ca/P ratio of 1.5, the tricalcium phosphate phase was dominant. However, small amounts of hydroxyapatite started to appear. For samples with Ca/P ratio of 1.67, the hydroxyapatite phase was dominant. Lastly, for samples with the Ca/P ratios of 2.0 and 2.5, the CaO phase started to appear in addition to the hydroxyapatite phase which was the dominant phase. Moreover, the average grain size, porosity (%) and the average pore size decreased with increasing the Ca/P ratios.

Keywords: Calcium phosphates; Bioceramics; Orthopedic implants; Characterization

1. Introduction

Calcium phosphates (CaPs) have been widely used as bulk implants or as coatings in biomedical applications to obtain improved bonding between bone and an implant [1]. CaPs may degrade in body fluids due to an acidic wound healing response and/or by cellular activity at low pHs [2]. Therefore, the release of CaP ions after the implantation influences the CaP coating stability and strength at the bone and a metal implant coated with a CaP [3]. Importantly, the long term stability of CaPs depends on their calcium (Ca) to phosphorous (P) ratios. Moreover, the Ca/P ratios of CaPs vary depending on the presence of phases which are α and/or β-tricalcium phosphate (TCP), tetracalcium phosphate, octacalcium phosphate ($Ca_2P_2O_7$), and hydroxyapatite (HA, $Ca_{10}(PO_4)_6(OH)_2$). Moreover, more amorphous CaPs (such as TCP) degrade much faster than the crystalline HA [4]. Among these phases, pure HA is the most stable and strongest phase when compared with other phases [5]. Moreover, doping ions have been added into structure of HA to improve the various properties of HAs [6–11].

Bone growth was significantly improved at the surface of an HA coated implant when compared to that on an uncoated implant [12]. However, more degradable CaPs may be more desirable in orthopedic applications such as drug delivery, bone grafting, and as biodegradable bone cement materials. Therefore, to improve the new bone formation rate, a biphasic HA/TCP ceramic was suggested to have improved values [13]. Moreover, many coating processes lead to bulk or localized Ca/P ratios that can deviate from the stoichiometric value of 1.67 for pure HA which could result in a lack of purity in the HA coating. Calcium oxide (CaO) can be obtained by either thermal decomposition or by additions of various chemicals to improve the thermal stability of the CaPs [14,15]. In addition to CaO, TCP could also form after the thermal decomposition of HA which may occur during the coating of HA on biometals.

* Corresponding author. Tel.: +90 212 2931300x2438; fax: +90 212 2450795.
E-mail address: ergunce@itu.edu.tr (C. Ergun).

0272-8842/$36.00
doi:10.1016/j.ceramint.2010.11.004

In vitro and in vivo biological responses to CaPs with various Ca/P ratios could produce fluctuation in biological responses of these materials in vitro or in vivo [16,17]. These biological responses mainly depend on the characteristics of the materials, such as their elemental composition, surface topography, porosity, density, shape and sizes [18,19]. Moreover, it is not easy to compare the published results regarding the variations on the test techniques, experimental set ups, etc. In previous studies, the CaPs with various Ca/P ratios were synthesized and characterized by different techniques [20–23]. For example, presence of phases in CaPs with Ca/P ratios of 1.00 and 1.54 was studied after the various heat treatments from room temperature to 1350 °C [20]. Therefore, in order to have a more complete understanding, it is very useful to make a comparative study to directly characterize the different samples to get more precise information about CaPs with various Ca/P ratios. The result of such comparative studies may be more dependable to choose appropriate CaP compositions for a specific biomedical application.

In this study, nano-size CaPs with a Ca/P molar ratio of 0.5, 0.75, 1.33, 1.5, 1.55, 1.67, 2, and 2.5 were synthesized for the first time by a precipitation method and sintered at 500 °C, 700 °C, 900 °C, 1100 °C and 1300 °C for 2 h. Synthesized CaPs were characterized by density measurements, X-ray diffraction (XRD) and scanning electron microscopy (SEM) equipped with an energy dispersive spectroscopy (SEM–EDS).

2. Experimental methods

CaPs were synthesized with a precipitation method [5]. Calcium nitrate tetra hydrate ($Ca(NO_3)_2{\cdot}4H_2O$) and di-ammonium hydrogen phosphate ($(NH_4)_2HPO_4$) were used as the main precursors. They were separately dissolved in distilled water. Then, the two solutions were mixed with different Ca/P ratios at a pH level of 11–12. The final mixture was then stirred for about 2 days. Then, the mixture was filtered with fine filter paper and a wet cake was obtained. The wet cake was dried in an oven at 60 °C for several days. The precipitated CaPs were crushed with an agate mortar and pestle, and the resulting powder sieved to obtain a mean particle size less than 75 μm in diameter. Cylindrical pellets were made from this powder by cold pressing at a pressure of 150 MPa. Finally, the samples were sintered in air at 500 °C, 700 °C, 900 °C, 1100 °C and 1300 °C for 2 h. The sample identification numbers and their relationship to Ca/P ratio of the samples are presented in Table 1.The phases of the samples were determined by XRD using a Rigaku Rint Dmax 100 machine. XRD was performed on the samples with a Cu-Kα radiation at 40 kV/30 mA with a scanning angle from 24° to 40° in 2θ with a scan speed of 2.0°/min. The XRD scan range was chosen between 24 and 40° because most of the CaP phases have the highest peaks between these ranges. Using the comparison of the positions of the diffracted planes obtained from the XRD results, Joint Committee on Powder Diffraction Standard (JCPDS) files were used to determine the presence of the phases.

SEM images and elemental analysis were obtained with a Philips XL30 FEG SEM. Quantitative image analysis techniques were used to determine the grain size, porosity and pore size of all samples from SEM micrographs. The linear intercept method was used to determine the average grain size of the CaPs sintered at 1100 °C for 2 h [24]. The area analysis technique was used to obtain the porosity and the average pore size of various CaP samples.

Table 1
Calcium phosphate sample abbreviations and their relationship to Ca/P ratio of the samples.

Sample abbreviation	Ca/P ratio
CaP050	0.50
CaP075	0.75
CaP133	1.33
CaP150	1.50
CaP155	1.55
CaP167	1.66
CaP200	2.00
CaP250	2.50

3. Results and discussion

XRD patterns of CaP050 are presented in Fig. 1. X-ray peaks of as precipitated phase matches to the JCPDS main standard peak group of HA (JCPDS#: 09-0432). However, presence of HA phase after the sintering cannot be concluded because the stoichiometric HA has a Ca/P ratio of 1.67. The wide peaks should be due to very small precipitate size of the precipitated CaP. At the sintering temperatures between 500 °C and 700 °C,

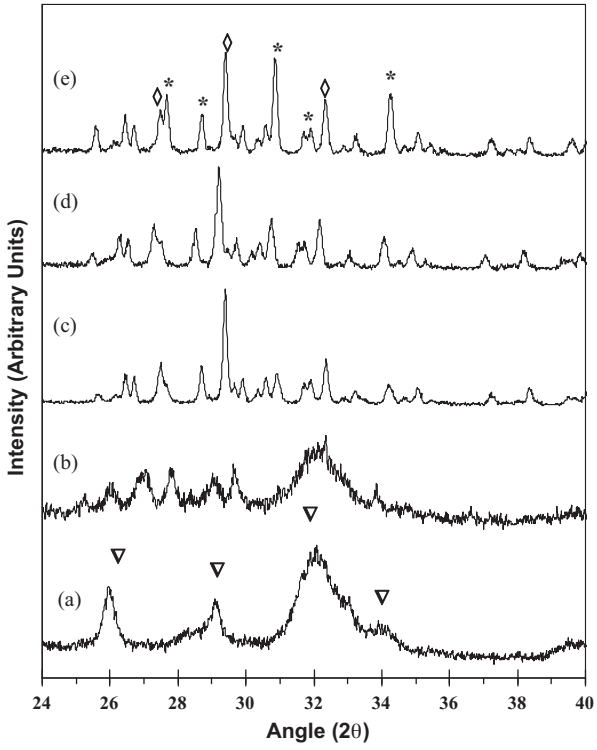

Fig. 1. XRD patterns of CaP050 samples: (a) as precipitated and sintered in air at: (b) 500 °C; (c) 700 °C; (d) 900 °C; (e) 1100 °C (▽, as precipitated HA; ▪, crystallized HA; *, β-TCP; ◇, $Ca_2P_2O_7$).

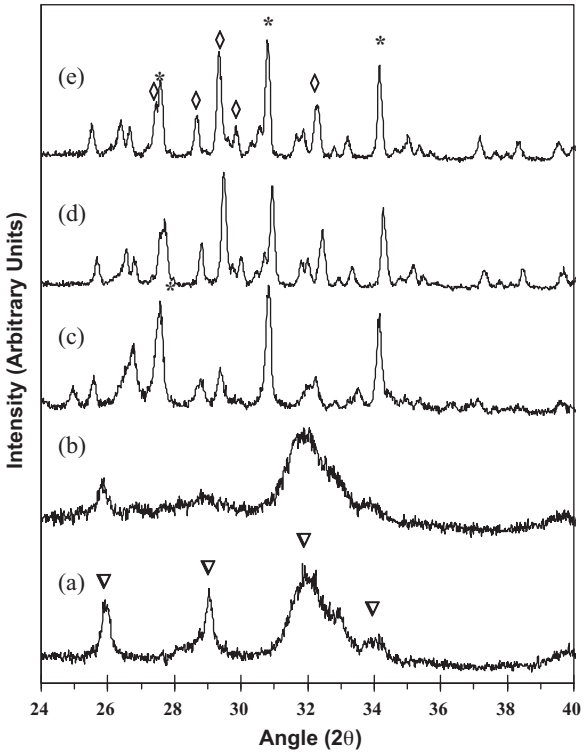

Fig. 2. XRD patterns of CaP075 samples: (a) as precipitated and sintered in air at: (b) 500 °C; (c) 700 °C; (d) 900 °C; (e) 1100 °C (▽, as precipitated HA; ▪, crystallized HA; *, β-TCP; ◇, $Ca_2P_2O_7$).

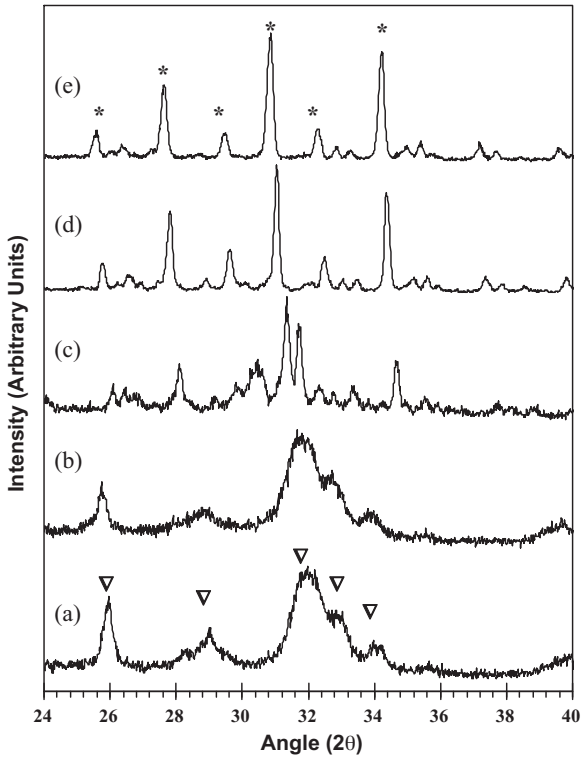

Fig. 3. XRD patterns of CaP133 samples: (a) as precipitated and sintered in air at: (b) 500 °C; (c) 700 °C; (d) 900 °C; (e) 1100 °C (▽, as precipitated HA; ▪, crystallized HA; *, β-TCP).

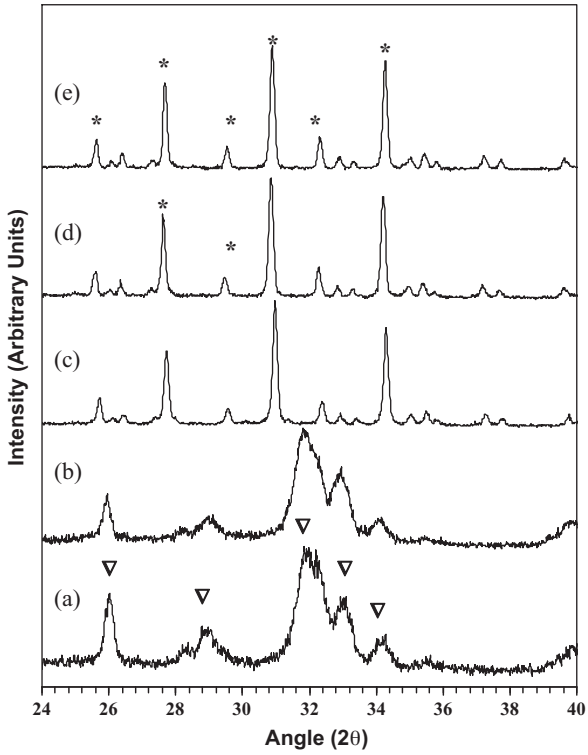

Fig. 4. XRD patterns of CaP150 samples: (a) as precipitated and sintered in air at: (b) 500 °C; (c) 700 °C; (d) 900 °C; (e) 1100 °C (▽, as precipitated HA; ▪, crystallized HA; *, β-TCP).

the precipitated phase started to partially transform to β-TCP (JCPDS#: 9-169) and $Ca_2P_2O_7$ in the sample CaP050. This transformation completed at 700 °C and all precipitated HA completely disappeared. The resulting phases of TCP and $Ca_2P_2O_7$ became fully crystallized in between 900 °C and 1100 °C indicated with the sharp TCP and $Ca_2P_2O_7$ peaks.

XRD patterns of the samples CaP075, CaP133, CaP150, CaP155, CaP167, CaP200, and CaP250 are presented in Figs. 2–8. Similar to CaP050, the precipitated phase was HA with very small crystallites in all CaP samples. The precipitates were transformed to other phases and fully crystallized after the sintering between 500 °C and 700 °C.

As seen in the XRD graph of the sample CaP075 in Fig. 2, the precipitated phase of HA started to transform into TCP and $Ca_2P_2O_7$ above the sintering temperature of 500 °C in a similar manner to CaP050. This transformation was completed at 700 °C. However, when we compared the ratio of the highest peak heights of TCP and $Ca_2P_2O_7$, the amount of TCP increased while that of $Ca_2P_2O_7$ decreased with increasing the Ca/P ratio from 0.50 to 0.75.

The samples: CaP133 and CaP150 showed almost a similar behavior as seen in Figs. 3 and 4, respectively. In both of the samples, the phase transformation of the as precipitated HA phase occurred between the sintering temperatures of 500 °C and 700 °C. However, the only stable phase was TCP. All precipitated HA disappeared. There was no $Ca_2P_2O_7$ phase present in these samples with Ca/P ratios of 1.33 and 1.50.

As seen in the XRD patterns of the sample CaP155 in Fig. 5, after the transformation of the precipitated phase after the

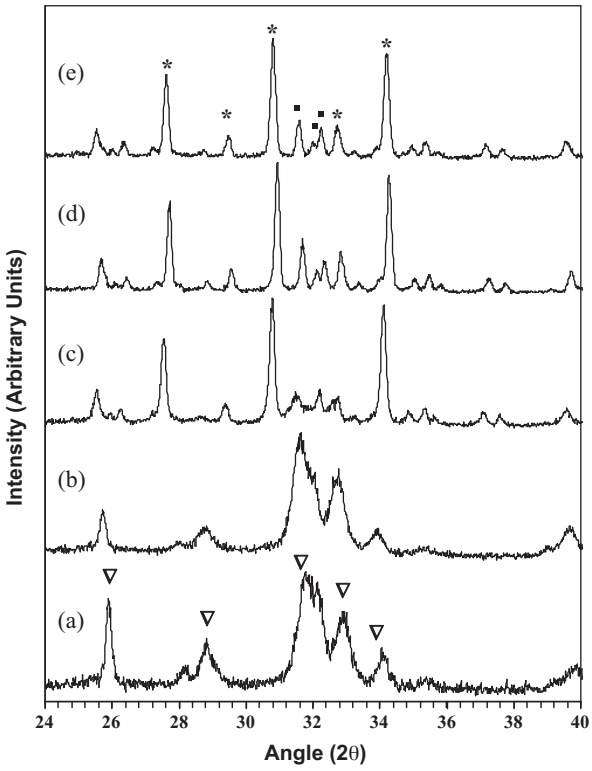

Fig. 5. XRD patterns of CaP155 samples: (a) as precipitated and sintered in air at: (b) 500 °C; (c) 700 °C; (d) 900 °C; (e) 1100 °C (▽, as precipitated HA; ▪, crystallized HA; *, β-TCP).

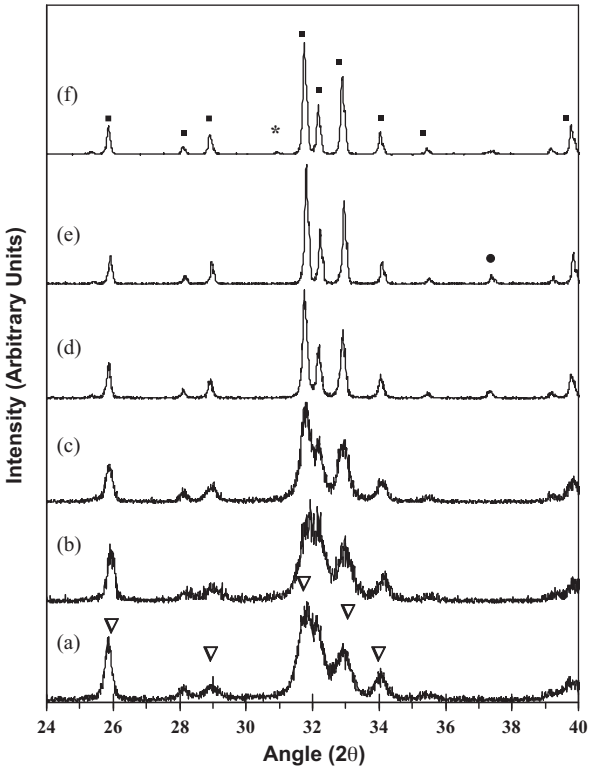

Fig. 7. XRD patterns of CaP200 samples: (a) as precipitated and sintered in air at: (b) 500 °C; (c) 700 °C; (d) 900 °C; (e) 1100 °C; (f) 1300 °C (▽, as precipitated HA; ▪, Crystallized HA; ●, CaO).

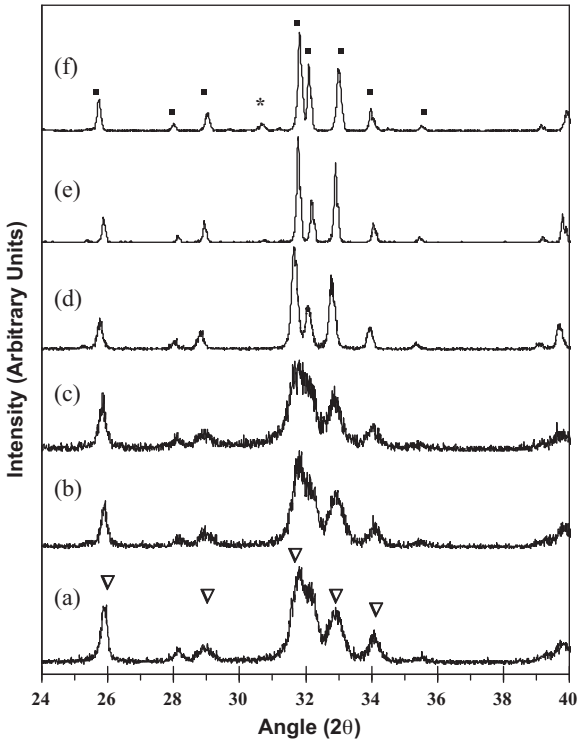

Fig. 6. XRD patterns of CaP167 samples: (a) as precipitated and sintered in air at: (b) 500 °C; (c) 700 °C; (d) 900 °C; (e) 1100 °C; (f) 1300 °C (▽, as precipitated HA; ▪, crystallized HA).

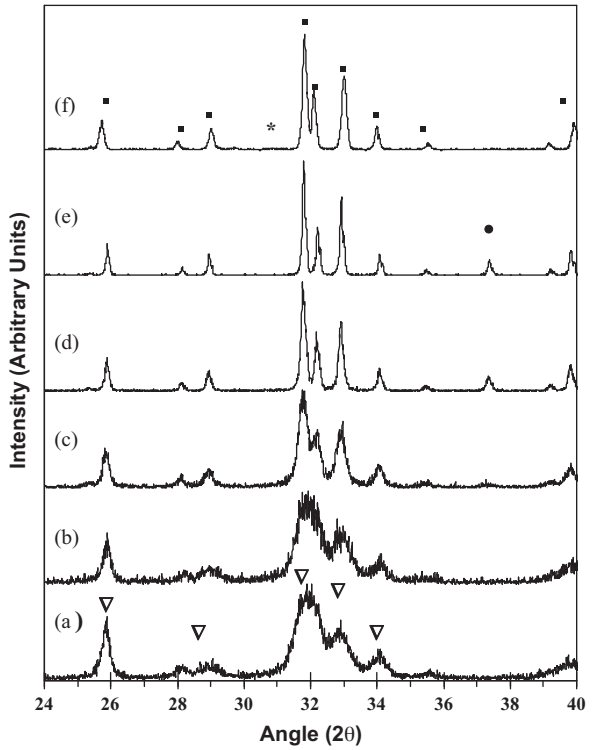

Fig. 8. XRD patterns of CaP250 samples: (a) as precipitated and sintered in air at: (b) 500 °C; (c) 700 °C; (d) 900 °C; (e) 1100 °C; (f) 1300 °C (▽, as precipitated HA; ▪, crystallized HA; ●, CaO).

sintering between 500 °C and 700 °C, the major stable phase was TCP. Moreover, a small amount of HA was also observed. As a result, a biphasic HA/TCP structure was observed. In the previous studies, it was shown that biphasic HA and TCP ceramics showed improved properties than the single phase of HA or TCP [22].

In the sample CaP167, the precipitated phase completely transformed into crystallized HA after the sintering between 500 °C and 700 °C as seen in Fig. 6. No other phases were observed. After the sintering of this sample at 900 °C and 1100 °C, pure HA was observed. Because this sample had the optimum Ca/P ratio of 5/3 to produce pure HA. However, upon sintering at 1300 °C, a small amount of TCP was observed due to the relatively high sintering temperature and the decomposition of HA into TCP. Because it was found that the optimum sintering temperature of 1100 °C and sintering time of

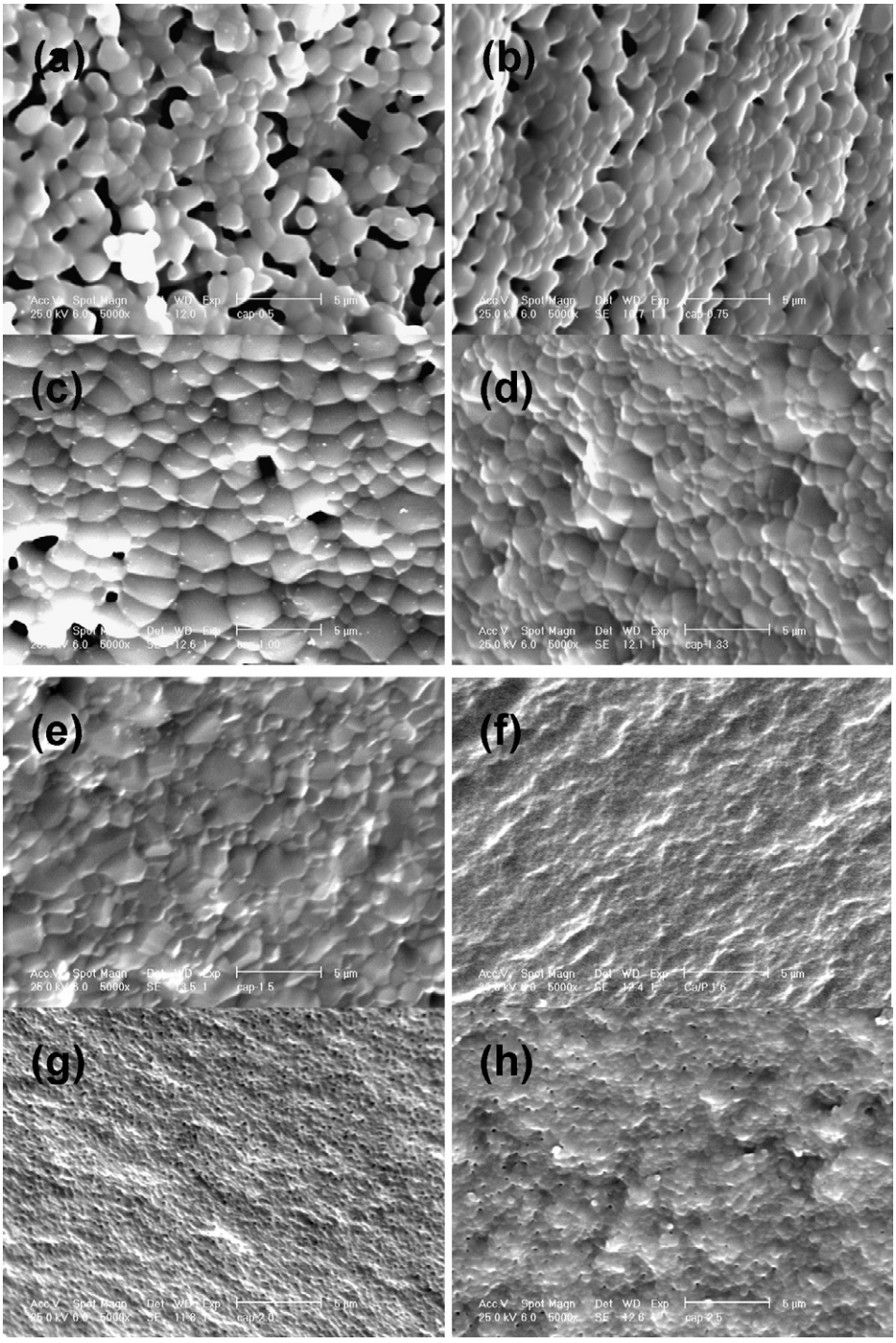

Fig. 9. SEM micrographs of the CaPs sintered at 1100 °C for 2 h: (a) CaP050; (b) CaP075; (c) CaP133; (d) CaP150; (e) CaP155; (f) CaP167; (g) CaP200; and (h) CaP250. Scale bars: 5 μm.

Table 2
Composition, grain size, amount of porosity and pore size in the CaP samples after the sintering at 1100 °C for 2 h.

Sample I.D. #	Composition (At.%)			Grain size (nm)	% porosity	Pore size (nm)
	Ca	P	O			
CaP050	45.15	24.96	29.89	1370	14.8	1010
CaP075	28.12	20.31	51.57	1300	7.2	630
CaP133	26.24	18.8	54.95	1830	6.2	580
CaP150	32.46	22.07	45.47	1437	3.3	410
CaP155	27.88	19.34	52.78	819	3.1	380
CaP167	36.34	22.8	40.86	290	2.9	260
CaP200	48.77	18.59	32.64	262	4.9	190
CaP250	36.01	14.96	49.04	575	3.3	220

1 h were found to obtain a pure HA which was synthesized by a precipitation method [5]. After the sintering of HA above 1100 °C, HA phase starts to decompose to TCP and CaO [5].

Presence of phases in the samples of CaP200 and CaP250 from the XRD graphs showed almost a similar behavior as shown in Figs. 7 and 8, respectively. As similar to other Ca/P ratios, the phase transformation in the as precipitated HA to other phases occurred after the sintering between 500 °C and 700 °C. After this transformation, although the major stable phase was crystalline HA, a small amount of CaO phase was also observed because of the presence of excess Ca^{2+} ions present in the system. Comparing the ratios of the characteristic peaks of HA and CaO, the amount of CaO in CaP250 was higher than that in CaP200. It should also be emphasized that no TCP or other decomposition phase was obtained in the sample CaP250 after the sintering at 1300 °C. This may be due to presence of CaO that increased the thermal stability of HA in these samples. As discussed earlier, CaO may be present in HA, as a byproduct of thermal decomposition or as intentional additions to improve the thermal stability of HA [5,14–17,19,25,26].

The SEM images of the samples sintered at 1100 °C for 2 h are shown in Fig. 9. From these SEM images, it was concluded that the average grain sizes, porosity and the average pore sizes of the samples decreased in general while Ca/P ratios increased (Table 2 and Fig. 9). The smaller grain sizes with increasing Ca/P ratios of the CaPs could probably be happened from coalescence of the particles with decreasing Ca/P ratios of the CaPs [27]. For example, CaP050 had grain sizes of 1370 nm, porosity of 14.8%, and pore sizes of 1010 nm while CaP250 had grain sizes of 575 nm, porosity of 3.3% and pore sizes of 220 nm, respectively.

Large pores and big grains seem to be associated with the low Ca/P ratios as observed particularly in the ratios of 0.5 and 0.75. As the concentration of this phase decreased with increasing the Ca/P ratio, porosity and grain sizes considerably decreased. In addition to the increased porosity and large grain sizes, the existence of $Ca_2P_2O_7$ phase provides the samples having Ca/P ratios of 0.5 and 0.75 a great potential as an in vivo biodegradable bone substitute [28,29].

The information given in this study could be useful in designing the CaP materials for orthopedic implant coatings, drug delivery applications, and degradable bone cements. For example, while HA is the most stable phase to create a bioactive coating on a metallic implant, the highest Ca/P ratio in CaPs would promote osteoblast adhesion the most. Similarly, for ceramic drug delivery applications, less crystalline materials are more desirable to degrade and release embedded bone building agents. Therefore, amorphous materials with the highest Ca/P ratios would promote osteoblast adhesion on those substrates.

The material properties such as decreased grain size and decreased porosity and pore size could alter the surface energetics, area and degree of nano-scale surface roughness. Specifically, quantitative analysis of SEM images revealed that for an increase in Ca/P ratio, smaller nanometer grain sizes were obtained by a decrease in porosity and pore size. In this manner, increased osteoblast adhesion on CaPs with smaller nanometer grain sizes has shown greater osteoblast adhesion, proliferation, alkaline phosphatase synthesis, and calcium deposition on pure HA with 67 compared to 167 nm grain sizes in previous studies [16,17,30]. Therefore, biological properties of these materials should be investigated in more detail.

4. Conclusions

In this study, the precipitated form of CaPs synthesized with a precipitation method was always HA with very small particle size and/or partial disorderness regardless of the Ca/P ratios in the starting precipitating condition. However, depending on the stoichiometry, this precipitated form was transformed into different CaP phases in the temperatures between 500 °C and 700 °C. When the Ca/P ratio is kept between 0.5 and 0.75, two different phases formed: β-TCP and $Ca_2P_2O_7$. When Ca/P ratio is kept between 1.33 and 1.50, the only stable phase was β-TCP. When Ca/P ratio was 1.55, slight amount of HA formation was observed while a ratio of 1.67 yielded a complete HA as the only stable phase. For the Ca/P ratio of 2.0, the formation of CaO was detected. The amount of this phase increased when the ratio increased to 2.5, Finally, when the Ca/P ratio increased in the samples, the following phases of β-TCP + $Ca_2P_2O_7$ → β-TCP → β-TCP + HA → HA → HA + CaO were observed after the sintering at high temperatures.

Acknowledgements

This work is supported by Istanbul Technical University-BAP program (Project no: 30803) and the Scientific & Technological Research Council of Turkey-BAYG program.

References

[1] R.H. Doremus, Review: bioceramics, J. Mater. Sci. 27 (1992) 285–297.
[2] L.L. Hench, R.J. Splinter, W.C. Allen, T.K. Greenlee, Bonding mechanisms at the interface of ceramic prosthetic materials, J. Biomed. Mater. Res. 5 (1971) 117–141.
[3] A. Jean, J. Pouezat, O. Laboux, D. Marion, G. Daculsi, Bone implant interface, in: P.J. Doherty (Ed.), Advances in Biomaterials, vol. 10, Elsevier, London, UK, 1993.
[4] C.P. Klein, A.A. Driessen, K. de Groot, A. van den Hooff, Biodegradation behavior of various calcium phosphate materials in bone tissue, J. Biomed. Mater. Res. 17 (1983) 769–784.
[5] M. Jarcho, C.H. Bolen, M.B. Thomas, J. Bobick, J.F. Kay, R.H. Doremus, Hydroxylapatite synthesis and characterization in dense polycrystalline form, J. Mater. Sci. 11 (1976) 2027–2035.
[6] Z.P. Sun, B. Ercan, Z. Evis, T.J. Webster, Structural, mechanical and osteocompatibility properties of Mg^{2+}/F^{-} doped nanophase hydroxyapatite, J. Biomed. Mater. Res. Part A 94A (2010) 806–815.
[7] T.J. Webster, E.A. Massa-Schlueter, J.L. Smith, E.B. Slamovich, Osteoblast response to hydroxyapatite doped with divalent and trivalent cations, Biomaterials 25 (2004) 2111–2121.
[8] C. Ergun, T.J. Webster, R. Bizios, R.H. Doremus, Hydroxylapatite with substituted Mg, Zn, Cd, and Y: structure and microstructure, J. Biomed. Mater. Res. 59 (2002) 305–311.
[9] T.J. Webster, C. Ergun, R.H. Doremus, R. Bizios, Hydroxylapatite with substituted Mg, Zn, Cd, and Y: mechanisms of enhanced osteoblast adhesion, J. Biomed. Mater. Res. 59 (2002) 312–317.
[10] B. Basar, Z. Evis, Structural investigation of nano hydroxyapatite doped with Y^{3+} and F^{-} ions, Mater. Sci. Technol. 25 (2009) 794–798.
[11] C. Ergun, Effect of Ti substitution on the structure of hydroxylapatite, J. Eur. Ceram. Soc. 28 (2008) 2137–2149.
[12] M. Stewart, J.F. Welter, V.M. Goldberg, Effect of hydroxyapatite/tricalcium-phosphate coating on osseointegration of plasma sprayed titanium alloy implants, J. Biomed. Mater. Res. A 69A (2004) 1–10.
[13] E.A. dos Santos, A.B.R. Linhares, A.M. Rossi, M. Farina, G.A. Soares, Effects of surface undulations of biphasic calcium phosphate tablets on human osteoblast behavior, J. Biomed. Mater. Res. A 74A (2005) 315–324.
[14] J. Cihlar, A. Buchal, M. Trunec, Kinetics of thermal decomposition of hydroxyapatite bioceramics, J. Mater. Sci. 34 (1999) 6121–6131.
[15] A. Tampieri, G. Celotti, S. Sprio, C. Mingazzini, Characteristics of synthetic hydroxyapatites and attempts to improve their thermal stability, Mater. Chem. Phys. 64 (2000) 54–61.
[16] C. Ergun, H. Liu, T.J. Webster, E. Olcay, S. Yılmaz, F.C. Sahin, Increased osteoblast adhesion on nanoparticulate calcium phosphates with higher Ca/P ratios, J. Biomed. Mater. Res. 85A (2008) 236–241.
[17] H. Liu, H. Yazici, C. Ergun, T.J. Webster, H. Bermek, An in vitro evaluation of the Ca/P ratio for the cytocompatibility of nano-to-micron particulate calcium phosphates for bone regeneration, Acta Biomater. 4 (2008) 1472–1479.
[18] G.P.A.T. Klein, K. de Groot, A.A. Driessen, H.B.M. van der Lubbe, A comparative study of different β-whiUockite ceramics in rabbit cortical bone with regard to their biodegradation behaviour, Biomaterials 7 (1986) 144–146.
[19] N.K. Wood, E.J. Kaminski, R.J. Oglesby, The significance of implant shape in experimental testing of biological materials: disc vs. rod, J. Biomed. Mater. Res. 4 (1970) 1–12.
[20] M. Maciejewski, T.J. Brunner, S.F. Loher, W.J. Stark, A. Baiker, Phase transitions in amorphous calcium phosphates with different Ca/P ratios, Thermochim. Acta 468 (2008) 75–80.
[21] S. Raynaud, E. Champion, D. Bernache-Assollant, P. Thomas, Calcium phosphate apatites with variable Ca/P atomic ratio. I. Synthesis, characterization and thermal stability of powders, Biomaterials 23 (2002) 1065–1072.
[22] S Kannan, J.H.G. Rocha, J.M.G. Ventura, A.F. Lemos, J.M.F. Ferreira, Effect of Ca/P ratio of precursors on the formation of different apatitic ceramics—an X-ray diffraction study, Scripta Mater. 53 (2005) 1259–1262.
[23] O.E. Petrov, E. Dyulgerova, L. Petrov, R. Popova, Characterization of calcium phosphate phases obtained during the preparation of sintered biphase Ca–P ceramics, Mater. Lett. 48 (2001) 162–167.
[24] J.E. Hillyard, J.W. Cahn, An evaluation of procedures in quantitative metallography for volume fraction analysis, Trans. Metall. Soc. AIME 221 (1961) 344–352.
[25] S.R. Taylor, D.F. Gibbons, Effect of surface texture on the soft tissue response to polymer implants, J. Biomed. Mater. Res. 17 (1983) 205–227.
[26] G. Muralithran, S. Ramesh, The effects of sintering temperature on the properties of hydroxyapatite, Ceram Int. 26 (2000) 221–230.
[27] S. Raynaud, E. Champion, D. Bernache-Assollant, Calcium phosphate apatites with variable Ca/P atomic ratio. II. Calcination and sintering, Biomaterials 23 (2002) 1073–1080.
[28] F.-H. Lin, C.-C. Lin, C.-M. Lu, H.-C. Liu, J.-S. Sun, C.-Y. Wang, Mechanical properties and histological evaluation of sintered β-$Ca_2P_2O_7$ with $Na_4P_2O_7{\cdot}10H_2O$ addition, Biomaterials 16 (1995) 793–802.
[29] C.-C. Lin, C.-J. Liao, J.-S. Sun, H.-C. Liu, F.-H. Lin, Prevascularized bone graft cultured in sintered porous β-$Ca_2P_2O_7$ with 5 wt% $Na_4P_2O_7{\cdot}10H_2O$ addition ceramic chamber, Biomaterials 17 (1996) 1133–1140.
[30] T.J. Webster, C. Ergun, R.H. Doremus, R.W. Siegel, R. Bizios, Enhanced functions of osteoblasts on nanophase ceramics, Biomaterials 21 (2000) 1803–1810.